IMPACT OF FOULING ON THERMO-HYDRAULICS OF VISCOUS COOLERS

E. M. Ishiyama[1] and *D. I. Wilson[2]
[1]Heat Transfer Research Inc., Surrey Technology Centre, 40 Occam Road, Guildford, Surrey, GU2 7YG, UK
[2]Department of Chemical Engineering and Biotechnology, University of Cambridge, Philippa Fawcett Drive, Cambridge, CB3 0AS, UK (*diw11@cam.ac.uk)

ABSTRACT

Viscous flow coolers require special attention at the design stage because the flow can exhibit thermo-hydraulic channeling as a result of the coupling between fluid viscosity and the rate of heat transfer. The impact of fouling on the performance of such devices was investigated. The fouling rate in a viscous flow cooler was quantified using a semi-empirical model analysing the data for wax deposition from wax/kerosene solutions reported by Ghedamu et al. [1]. This was combined with a simulation of the flow cooler reported by Rohsenow et al. [2] which reproduced the thermo-hydraulic chanelling reported therein. It is shown that a reduction in pressure drop with fouling can occur as a result of poorer heat transfer and a smaller change in fluid viscosity. The behaviour is found to be determined by the deposit thermal conductivity: for values in the range expected for waxy deposits, fouling in tubes with different thermal resistance can have the same pressure drop for a given flow rate. Highly non-linear pressure drop-heat transfer behaviour can arise during the initial stages of fouling, which is noticeably different from that observed when deposit initially changes the roughness of the deposit.

INTRODUCTION

Viscous flow coolers are used in wide range of process applications including cooling of lube/fuel oils, effluent streams, surfactants, food processing, pharmaceuticals and polymers. A key concern in the design and operation of viscous coolers is flow maldistribution, which results in significant deterioration of thermal and flow performance [3]. There are mainly two classes of flow maldistribution as described by Rohsenow et al. [2]: (*i*) geometry-induced maldistribution and (*ii*) operation-induced maldistribution. This paper concerns the latter, particularly in relation to stream viscosity and fouling for a single pass shell-and-tube heat exchanger with the viscous fluid on the tube-side. A comprehensive review of flow maldistribution phenomena in heat exchangers has been presented by Mueller and Chiou [4].

The viscous stream being cooled can be on either the tube- or the shell-side of a shell-and-tube heat exchanger. Having the viscous stream on the shell-side is likely to enhance heat transfer, but care has to be taken to avoid the formation of dead and low velocity zones. Mueller [5] showed that when the viscous stream undergoes laminar flow on the tube-side of a single-pass exchanger, below a certain pressure drop limit two different flow rates can give the same pressure drop. The analysis was extended by Putnam and Rohsenow [6] for case studies on a Mobil aviation oil.

A similar effect was reported by Wonchala and Wynnyckyj [7] for cooling of gases passing through a hot packed bed. It stems from the decrease in the resistance to flow of a gas through a packing with decreasing temperature (as the viscosity decreases). Within a packing of uniform porosity, once a locally cold region is established, it becomes the favoured flow channel by virtue of its lower resistance.

In this manuscript the impact of fouling on a tube is explored to understand the interpretation of thermal-hydraulic performance data under fouling. It differs from themal-hydraulic channelling considered previously where fouling caused flow maldistribution *between* parallel heat exchangers [8].

Wax deposition model
There has been extensive research on wax deposition owing to its relevance to crude oil transport in subsea pipelines (e.g. [9–12]). The experimental data on wax deposition reported by Ghedamu [1,13] were revisited as their analysis focused on the asymptotic fouling resistance and not on the influence of operating conditions on the fouling rate. The heat transfer and hydraulic conditions of the annular test rig used by Ghedamu is evaluated and analysed in relation to the initial wax deposition rate. The experimental set up consisted of a single tube countercurrent annular test section (Figure 1), with cooling water passing through the inner tube and a solution of wax in kerosene in the annulus. A full description of the apparatus is given in [13].

To evaluate the surface temperature of the annular section at the start and completion of the

experiment, the heat transfer coefficient on the outer surface of the inner tube, h_{ann}, was estimated using the correlations reported by Gnielinski [14].

$$\frac{h_{ann}d_h}{k} = \frac{\left(\frac{f_{ann}}{8}\right)Re\,Pr}{k_1 + 12.7\sqrt{\frac{f_{ann}}{8}\left(Pr^{\frac{2}{3}}-1\right)}}\left[1+\left(\frac{d_h}{L}\right)^{\frac{2}{3}}\right]F_{ann}K \qquad (1)$$

Here Re is the Reynolds number, Pr the Prandtl number, d_h the hydraulic diameter, L the tube length, f_{ann} is the friction factor in an annulus, F_{ann} is a factor accounting for the dependence of a (where $a = d_i/d_o$, with d_i the outer diameter of the inner tube and d_o the inner diameter of the outer tube), k the fluid thermal conductivity. The Reynolds number Re is given by

$$Re = \frac{ud_h}{\nu} \qquad (2)$$

where u is the velocity and ν the kinematic viscosity.

Parameter k_1 is a function of Re and Pr, and K accounts for the temperature dependence of fluid properties. The parameters k_1, f_{ann}, F_{ann} and K are obtained *via*

$$k_1 = 1.07 + \frac{900}{Re} - \frac{0.63}{(1+10\,Pr)} \qquad (3)$$

$$f_{ann} = \left(1.8\,log_{10}\,Re^* - 1.5\right)^{-2} \qquad (4)$$

$$Re^* = Re\frac{\left(1+a^2\right)ln\,a + \left(1-a^2\right)}{\left(1-a\right)^2\,ln\,a} \qquad (5)$$

$$F_{ann} = 0.75\left(\frac{d_i}{d_o}\right)^{-0.17} \qquad (6)$$

$$K = \left(\frac{Pr}{Pr_{wall}}\right) \qquad (7)$$

The surface temperature, T_s, is obtained by solving the heat balance

$$Q = h_{ann}A_{ann}\left(T_b - T_s\right) \qquad (8)$$

where Q is the heat duty, A_{ann}, is the heat transfer area of the annulus and T_b is the bulk temperature. The uncertainty in the calculated surface temperature is estimated from

$$\left(\frac{\delta T_s}{T_s}\right)^2 = \left(\frac{\delta T_b}{T_b}\right)^2 + \left(\frac{\delta Q}{Q}\right)^2 + \left(\frac{\delta h_{ann}}{h_{ann}}\right)^2 + \left(\frac{\delta A_{ann}}{A_{ann}}\right)^2 \qquad (9)$$

The shear stress on the outer surface of the inner tube, τ_i, was estimated using the methodology described by Bennett and Hohmann [15]:

$$\tau_i = \frac{\left(d_{max}^2 - d_i^2\right)}{4d_i}\left(\frac{f_a}{d_o - d_i}\right)\left(\frac{\rho u^2}{2}\right) \qquad (10)$$

Here u is the velocity, f_a is the annular friction factor, and d_{max} is the diameter of maximum velocity in the annular velocity profile.

$$f_a = \left(1 + 0.0925\left(\frac{d_i}{d_o}\right)\right)f_t \qquad (11)$$

$$f_t = 0.0014 + 0.125\,Re^{-0.32} \qquad (12)$$

$$d_{max} = \sqrt{\frac{d_o^2 - d_i^2}{2\,ln\left|\frac{d_o}{d_i}\right|}} \qquad (13)$$

with f_t the tube side friction factor.

Ghedamu investigated the impact of different surfaces on wax deposition. Two of the data sets, for fouling from 20 wt% slack wax/kerosene mixtures on 316 stainless steel surfaces are analysed. Dataset 1 consisted of experiments performed over a range of Reynolds numbers, with the average bulk temperature constant. Dataset 2 consisted of experiments for a range of bulk temperatures, keeping the average Reynolds number constant.

Data set 1
The impact of flow rate on wax deposition was examined at an average bulk temperature of 31.4 ± 0.3 °C, water velocity of 1.1 m/s and an average chilling water temperature of 10.4 ± 1.5 °C. The reported fouling resistance-time data obeyed Kern-Seaton (asymptotic) behaviour: the Reynolds number, Re, and fitted Kern-Seaton parameters (asymptotic resistance, R_f^*, time taken to reach the asymptotic resistance θ_c) for each run are summarized in Table 1. The asymptotic fouling resistance decreases with flow rate while the time to reach this level of deposition tends to increase with flow rate, with an exception at the largest value. It should be noted that the temperature at the interface of the fouling layer and the shear stress there will differ between each test.
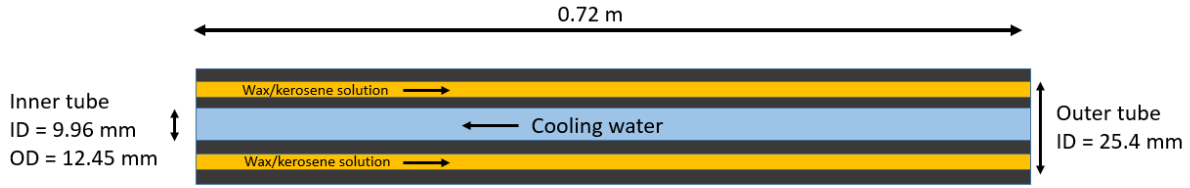
Figure 1: Schematic of wax fouling annular test section (based on Ghedamu [13]).

Table 1: Data set 1. Effect of flow rate, expressed as Reynolds number, on asymptotic fouling behaviour for 20 wt% slack wax/kerosene solution on stainless steel surfaces. The average T_b was 31.4 ± 0.3 °C.

Re	R_f^* (m²K/kW)	θ_c (min)
6650	0.929	8.0
8720	0.824	10.8
10600	0.793	13.2
12200	0.724	18.1
14400	0.667	10.3

The cloud point, T_{cloud}, of the wax/kerosene mixture was reported as 27.8 °C. The difference between T_{cloud} and T_s quantifies the driving force for wax deposition. Once T_s exceeds T_{cloud}, the wax will not precipitate. Figure 2 shows the difference between the cloud point and the surface temperature at the beginning and at the end of each test. The individual tests are presented in terms of the average wall shear stress, which increases with flow rate. The end of the experiment was defined by the fouling resistance reaching an asymptotic value (when no further wax buildup occurs). The plot shows that the end of deposition corresponds to the temperature difference approaching zero, within the bounds of uncertainty. At small temperature differences, the rate of growth will be very slow and it is postulated that the rheology of the wax crystal matrix may differ from that formed under faster growth conditions, affecting its response to shear stress imposed by the flow.

Based on a power law curve fit for the data set in Figure 3, the following expression is obtained:

$$\left(\frac{dR_f}{dt}\right)_{initial} = 0.0799\tau_i^{-0.583} \qquad (14)$$

Combining equations (16) and (14) gives the relationship

$$\left(\frac{dR_f}{dt}\right)_{initial} = 4.1\times10^{-4}\left(T_{cloud} - T_s\right)^{2.54} \qquad (15)$$

which can be used in the simulations. The shear stress is strongly linked to the surface temperature, hence $T_{cloud} - T_s$.

Figure 2 shows the non-linear linear fit obtained for the relationship between $(T_{cloud} - T_s)$ and τ_i at the start of the experiment:

$$\left(T_{cloud} - T_s\right)_{start} = 8.02\tau_i^{-0.23} \qquad (16)$$

Figure 3 gives the relationship between τ_i and the initial fouling rate, given by R_f^*/θ_c. The fouling rate is presented on the basis of a change in fouling resistance per minute scale.
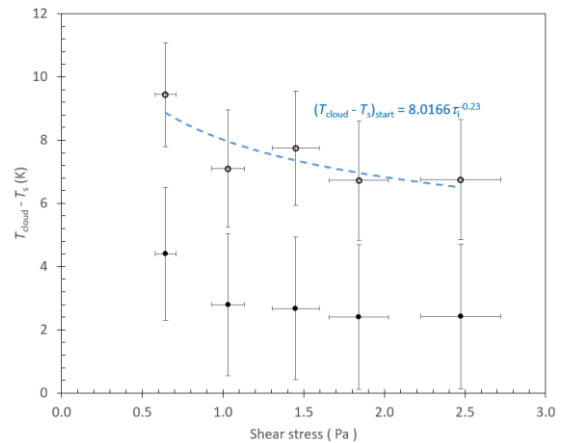
Figure 2: Data set 1. Difference between cloud point and calculated surface temperature. Open symbols - start of the experiment; solid symbols – end. Dashed locus shows fit to former.
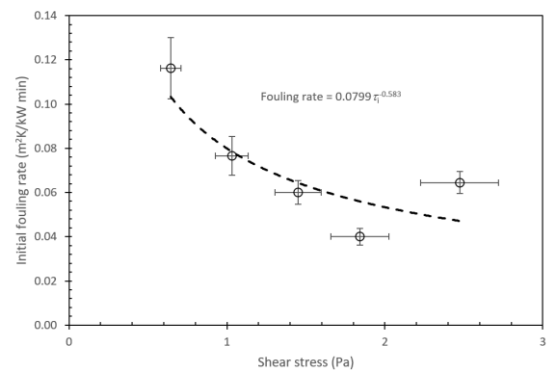
Figure 3: Effect of interface shear stress on initial fouling rate for Data set 1.

Data set 2
The impact of bulk temperature (average of inlet and outlet bulk temperature) of the kerosene/wax mixture on wax deposition was examined in tests featuring an average Reynolds number of 9430 ±

1170, water velocity of 1.1 m/s and an average bulk cooling water temperature of 7.9 ± 0.5 °C. The results are summarized in Table 2. The cloud point is the same as Data set 1 as the same slack wax mixture composition was used.

Table 2: Data set 2. Effect of bulk wax/kerosene solution temperature on asymptotic fouling behaviour under constant flow conditions

T_b	R_f*(m^{2}K/kW)	θc (min)
28.9	1.52	16.2
31.2	0.82	10.8
34.0	0.38	5.2
38.1	0.22	2.7
40.6	0.39	2.3
40.8	0.24	1.0

The initial fouling rate is plotted against $T_{cloud} - T_s$ in Figure 4. There is a general trend of fouling rate increasing with surface subcooling. The plot shows the trend obtained with Data set 1, equation (15). This agreement is fair: the same orders of magnitude are obtained but more work is required to identify a general fouling model. This is the subject of ongoing work, which includes analysis of other data sets reported by Ghedamu, including tests on surfaces other than stainless steel. Equation (15) offers a ball-park prediction which is used in the following case study. In due course the model should be replaced by one developed for these lower Reynolds number conditions.
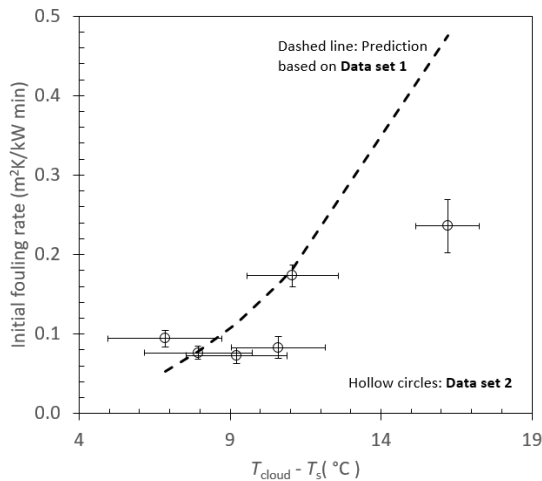
Figure 4: Effect of temperature driving force ($T_{cloud} - T_s$) on inital fouling rate. Symbols - experimental data from Data set 2. Dashed locus shows prediction using the relationship obtained for Data set 1, equation (15).

Case study

The case study is based on the aviation motor oil cooler example presented by Putnam and Rohsenow [6]. Their theoretical study consisted of a flow of aviation oil flowing along a circular tube cooler operating at constant wall temperature (Figure 5). The thermo-physical properties of the oil summarized in Table 3. The wax deposition dynamics from the Ghedamu work are employed to investigate the impact of wax deposition on the thermo-hydraulic performance of the cooler.

Table 3: Aviation motor oil properties

Parameter	Value
Density, ρ	881 kg m^{-3}
Specific heat capacity, C_p	2.09 kJ kg^{-1} K^{-1}
Thermal conductivity, k	0.138 W m^{-1} K^{-1}
Dynamic viscosity*	$\mu = c_1\, exp\left(-c_2 T\right)$ C_1 = 7.009 Pa s C_2 = − 0.074 °C^{-1}

* fitted to the graphical representation of the dynamic viscosity in Putnam and Rohsenow [6]. T in °C.
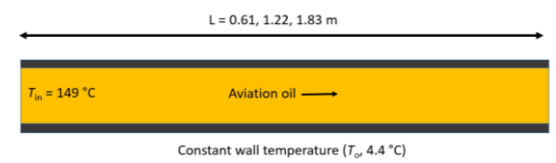
Figure 5: Schematic of constant wall temperature tube cooling aviation oil. Tube i.d. 63 mm.

Assuming plug flow, an enthalpy balance gives

$$wC_p dT = h\pi\left(d_i - 2\delta\right)\left(T - T_o\right)dx \qquad (17)$$

$$\frac{dT}{T - T_o} = \frac{\pi k}{wC_p}\left(\frac{h\left(d_i - 2\delta\right)}{k}\right)dx \qquad (18)$$

where w is the mass flow rate, C_p is the specific heat capacity, T is the mixed bulk fluid temperature as a function of length, h is the film transfer coefficient, d_i is the tube internal diameter, T_o is the wall temperature, x is the axial distance along the tube, δ is the deposit thickness and k is the fluid thermal conductivity.

The following equation describing the change in bulk temperature along the exchanger length is obained by combining equation (18) with the result for the Nusselt number in the entrance region of tubes with uniform wall temperature suggested by Kays [16]:

$$\frac{dT}{T-T_s} = \left(\frac{\mu_s}{\mu_b}\right)^n \left(3.66 + \frac{0.0668 \frac{4}{\pi x} \frac{wC_p}{k}}{1+0.04\left[\frac{4}{\pi x}\frac{wC_p}{k}\right]^{\frac{2}{3}}}\right) \frac{\pi k}{wC_p} dx \qquad (19)$$

Exponent n (accounting the change in Nusselt number for the variable viscosity over uniform viscosity case) was obtained by fitting to the data presented by Putnam and Rohsenow [6] for the effect of bulk temperature at constant wall temperature of 4.4 °C, giving

$$n = 0.515 T_b^{-0.353} \qquad (20)$$

where T_b is in °C. The change in pressure over increment dx is given by

$$\frac{dP}{dx} = \frac{64}{Re} \frac{1}{(d_i - 2\delta)} \frac{w^2}{2\rho} \qquad (21)$$

Accounting for the radial variation in temperature on the friction factor gives

$$\frac{dP}{dx} = \frac{64}{Re}\left(\frac{\mu_s}{\mu_b}\right)^m \frac{1}{D} \frac{w^2}{2\rho} \qquad (22)$$

The exponent m, accounting the change in friction factor for the variation in viscosity compared to a uniform viscosity case, was obtained by fitting to the data presented by Putnam and Rohsenow [6] for different bulk temperatures at a wall temperature of 4.4 °C, giving

$$m = -3.65\times10^{-8}T_b^3 + 1.455\times10^{-5}T_b^2 \\ - 2.624\times10^{-3}T_b + 0.5694 \qquad (23)$$

Giving, in integral form:

$$\Delta P = \frac{128}{\pi\rho(d_i - 2\delta)^4} w\int_0^L \mu_s^m \mu_b^{1-m} dx \qquad (24)$$

The predicted mixed cup temperature and pressure drop profiles at steady state for the flow conditions reported by Putnam and Rohsenow are presented in Figure 6 and Figure 7. These reproduce the profiles reported in their paper faithfully. The occurrence of multiple solutions delivering the same pressure drop is evident in Figure 7. The slow flow rate solution represents the case where the liquid cools significantly, resulting in a high viscosity.
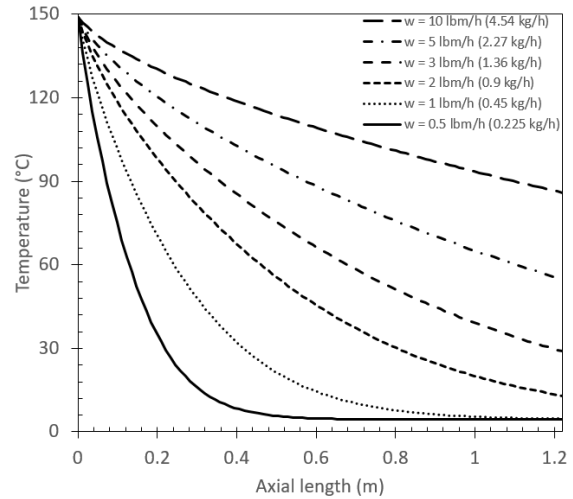
Figure 6: Case study, no fouling: predicted bulk temperature profiles for different flow rates.
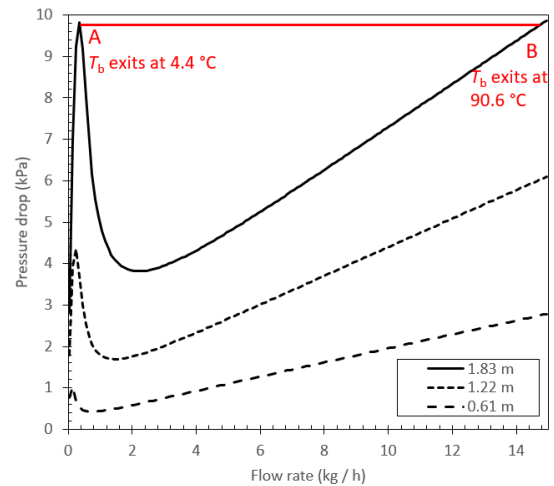
Figure 7: Case study, no fouling: predicted pressure drop profiles for a range of flow rates for three different tube lengths. Horizontal line for L = 1.83 m case indicates a pressure drop that is observed at two different flow rates, marked A and B.

In a multi-tube viscous cooler, the impact of flow maldistribution is poor overall heat transfer. Given the difference in the magnitude of the flows (*e.g.* for the 1.83 m tube case in Figure 7, A corresponds to a flow of ~ 0.5 kg/h while B is ~ 15 kg/h for a pressure drop of 9.8 kPa), an analysis of the overall rate of heat transfer indicates that that the contribution from the lower flow rate is small and flow maldistribution would be equivalent to blockage of tubes operating at the lower flow rate. The impact of fouling would then need to focus on tubes operating at the higher flow rate. The impact of fouling on such a tube with fouling given by equation (15) is now considered.

The overall heat transfer coefficient, U, is given by

$$\frac{1}{U} = \frac{1}{U_{cl}} + R_f \qquad (25)$$

where U_{cl} is its value under clean conditions and R_f is the fouling resistance. At time step t_n, R_f is given by

$$R_{f,t_n} = R_{f,t_{n-1}} + \frac{dR_f}{dt}\Delta t \qquad (26)$$

The deposit thickness δ is calculated using

$$\delta = \frac{d_i}{2}\left(1 - \frac{1}{exp\left(\frac{2\lambda R_f}{d_i}\right)}\right) \qquad (27)$$

where λ is the deposit thermal conductivity. The fouling Biot number, Bi_f, is defined thus:

$$Bi_f = R_f U_{cl} \qquad (28)$$

The impact of fouling was simulated for the case of $L = 1.22$ m and $w = 1$ kg h^{-1} and a range of λ values, 0.17 to 0.5 W m^{-1} K^{-1}, spanning the likely range, for a period of 6000 s.

The total heat transfer rate, Q, was obtained via performing incremental heat balance calculation along the tube length and obtaining the total *via*:

$$Q = \sum_{i=0}^{n} U_i A_i \left(T_{b,i} - T_s\right) \qquad (29)$$

Here, n is the number of increments and ΔA_i is the heat transfer area at increment i.

Figure 8 shows an example set of results for the flow radius and the surface temperature at selected times for a deposit thermal conductivity typical of an oil (0.2 W m^{-1} K^{-1}). Figure 8(a,iv)) shows that this condition is approached at the entrance to the tube, which features a combination of warm bulk fluid and high film heat transfer coefficient, after 600 s. Deposition occurs steadily elsewhere through the tube and the growth in deposit thickness results in an appreciable occlusion of flow area. $T_s(x)$ increases over time, resulting in falling fouling rate behavior and the heat duty, Q, decreases steadily over time. Figure 9 combines the plots in Figure 8 with an additional data set for 6000 s. At this time no new deposit is formed at the tube entry, where $T_s \geq T_{cloud}$.

Figure 10 summarises the predicted thermo-hydraulic behaviour for some thermal conductivities of interest. It can be seen that λ determines the thermo-hydraulic performance.

For deposits with higher thermal conductivity, (0.5 W m^{-1} K^{-1}) the pressure drop increases with fouling, as is often seen with other types of fouling. For lower λ values, near those expected for waxy deposits, strongly non-linear behaviour is observed. The pressure drop initially decreases and then increases, which is caused by the impact of reduced

heat transfer on viscosity: the fluid is not cooled to the same extent. For low values (< 0.19 W m^{-1} K^{-1}) the viscosity effect dominates and the pressure drop is always low. For intermediate values, there is a competition between thermal impact (lower viscosity) and duct constriction (higher mean velocity). In these cases, the same pressure drop can be associated with two different thermal duties and maldistribution of flow, promoting fouling, can be masked by these common pressure drops.

The drop in heat duty is greater for a higher deposit thermal conductivity (Figure 10 (b)) as the deposit surface temperature will be closer to the wall temperature, resulting in a larger rate of increase in thermal resistance predicted by the fouling model (equation 16).

Complex relationships between tubeside pressure drop and extent of fouling have been discussed previously (*e.g.* [17]), notably those arising from deposition of particulates which give rise to greater surface roughness. In that case, roughness increases the tubeside film heat transfer coefficient and Bi_f can initially be negative: with extended deposition, Bi_f becomes positive. The ratio $\Delta P/\Delta P_{cl}$ is always positive (for the constant throughput case), which is fundamentally different to the behaviour in Figure 9. To the authors' knowledge this has not been identified previously. This result emphasizes that fouling monitoring should be based on simultaneous pressure drop and thermal performance monitoring: the relationship between these data can provide valuable insights into the active fouling mechanisms.

Conclusions

Wax deposition data from Ghedamu's experiments were analysed and a simple relationship representing the wax deposition rate with the temperature driving force for deposition, $T_{cloud} - T_o$, is presented.

For viscous coolers, a reduction in pressure drop with fouling may arise due to the effect of reduced heat transfer on fluid viscosity. Tubes with different thermal resistances can exhibit the same pressure drop for the same flow rate.

The dimensionless pressure drop-thermal impact behaviour is determined by the deposit thermal conductivity. For values likely to apply to wax deposits, the dependency differs noticeably from the well-known roughness effect. Fouling can exacerbate thermal-hydraulic channeling in these devices.
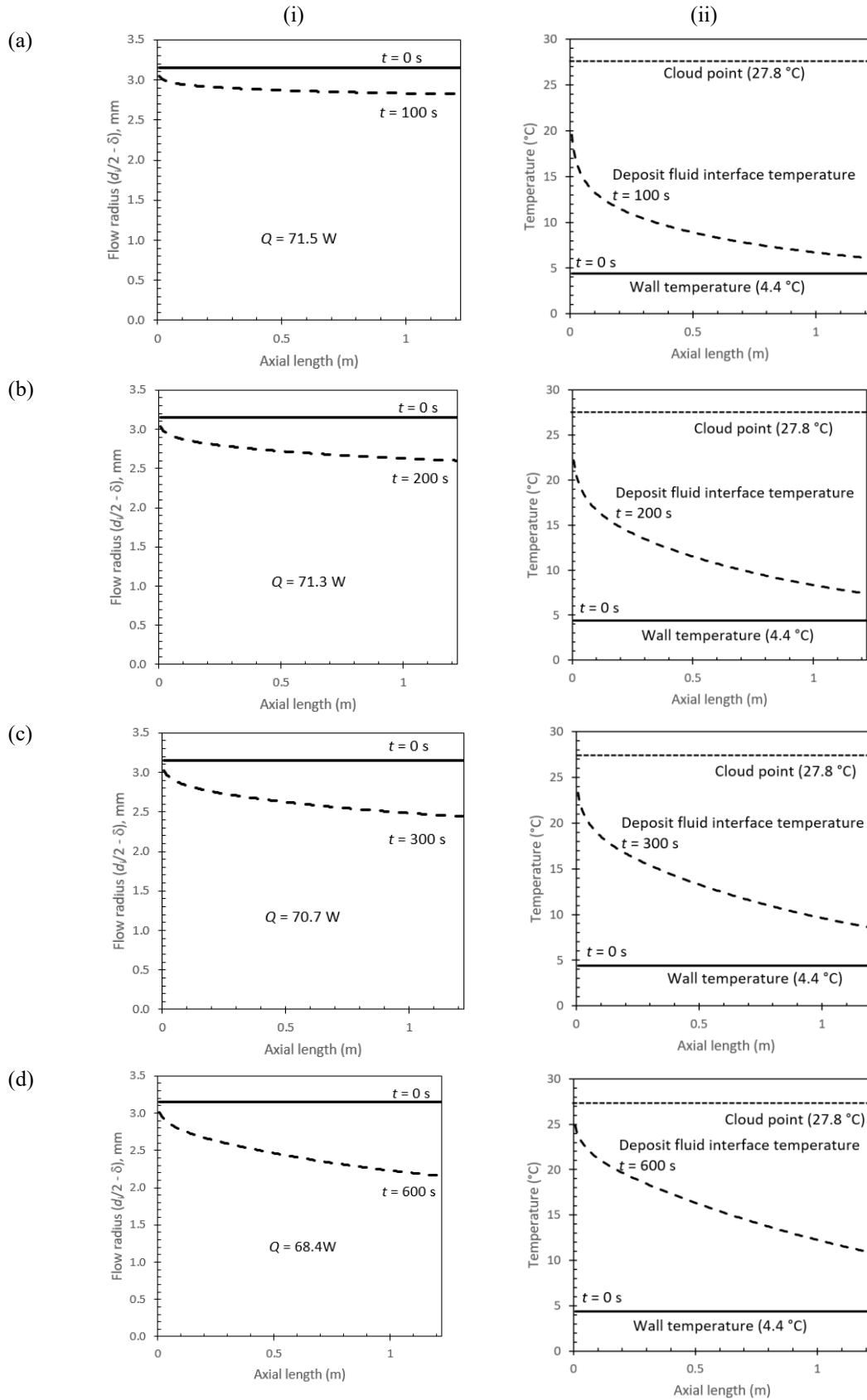
Figure 8: Simulated (*i*) flow radius and (*ii*) surface temperature profiles at times (*a*) 100 s, (*b*) 200 s, (*c*) 300 s and (*d*) 600 s for a deposit thermal conductivity of 0.2 W m^{-1} K^{-1}. Total duty Q indicated on (i).
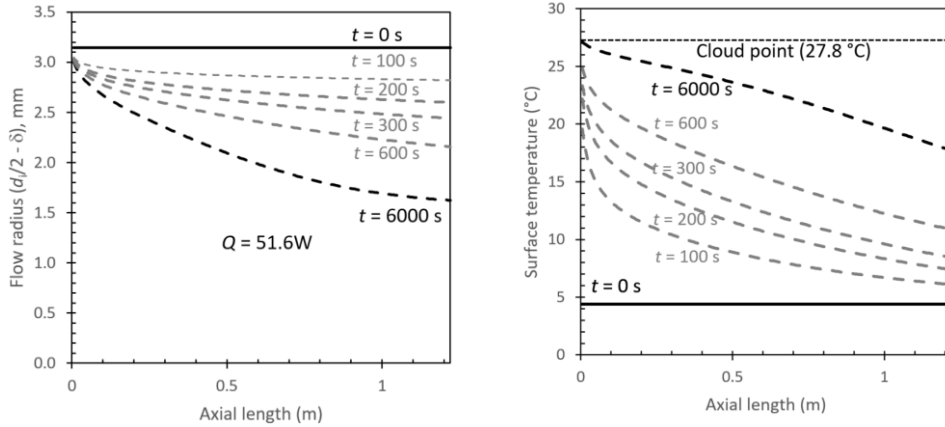
Figure 9: Summary of (*i*) flow radius and (*ii*) surface temperature profiles at times 100 s, 200 s, 300 s 600 s and 6000s for a deposit thermal conductivity of 0.2 W m^{-1} K^{-1}.
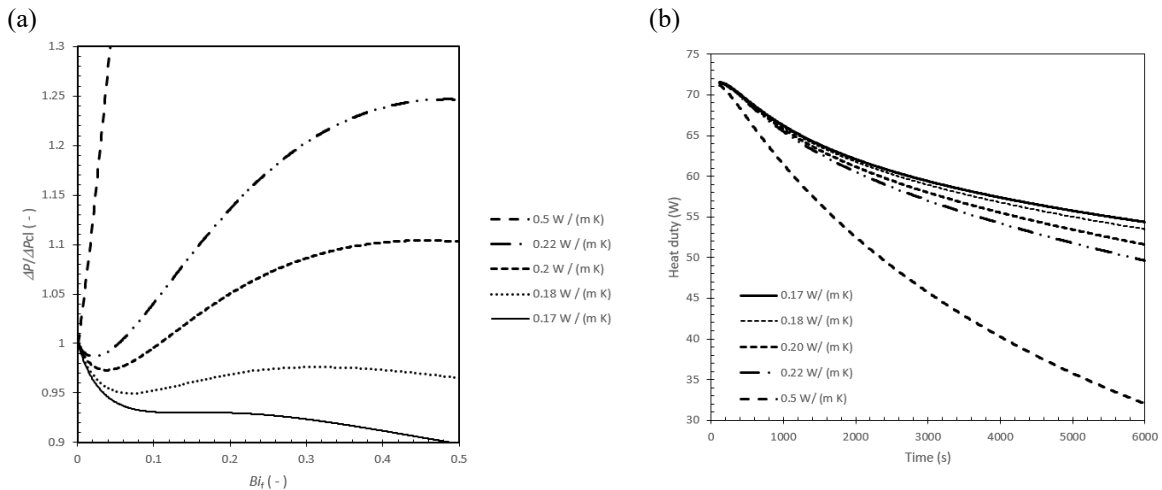
Figure 10: Effect of deposit thermal conductivity on (a) relationship between hydraulic penalty ($\Delta P/\Delta P_{cl}$) and thermal penalty (expressed as Bi_f) and (b) evolution of heat duty for constant throughput case study.

Nomenclature

A_{ann} heat transfer area of the annulus, m^2
c_1 constant in viscosity correlation, Pa s
c_2 constant in viscosity correlation, °C^{-1}
C_p specific heat capacity, J kg K^{-1}
d_h hydraulic diameter, m
d_i outer diameter of the inner tube for annulus, inner diameter of a plain tube, m
d_{max} diameter of maximum velocity, m
d_o inner diameter of the outer tube, m
f_a friction factor of an annulus (for shear stress), -
f_{ann} friction factor of an annulus (for heat transfer), -
F_{ann} factor accounting the dependence of d_i/d_o, -
f_t friction factor of a tube, -

h film transfer coefficient, W m^{-2}K^{-1}
h_{ann} heat transfer coefficient on the outer surface of the inner tube, W m^{-2}K^{-1}
k fluid thermal conductivity, W m^{-1}K^{-1}
K parameter accounting the temperature dependence on the fluid properties,
k_1 function of Re and Pr, -
L length of the tube, m
m exponent for viscosity dependence (ΔP), -
n exponent for viscosity dependence (Q), -
Pr Prandtl number, -
Q heat duty, W
Re Reynolds number, -
R_f fouling resistance, m^{2}K kW^{-1}, m^{2}K W^{-1}
R_f^* asymptotic fouling resistance, m^{2}K kW^{-1}

t time, s
T average mixed fluid temperature, K
T_o wall temperature, K
T_b average mixed temperature, K
T_{cloud} cloud point, K
T_s surface temperature, K
u velocity, m/s
U overall heat transfer coefficient, $W\ m^{-2}\ K^{-1}$
w mass flow rate, $kg\ s^{-1}$
x length along the exchanger, m

Symbols
δ deposit thickness, m
ΔP pressure drop, Pa
θ time taken to reach the asymptote, s
μ dynamic viscosity, Pa s
τ_i shear stress on annulus inner tube outer wall, Pa

Subscripts
b   average mixed condition
cl   clean condition
initial initial condition
n   at time step n
o   at the wall

References

[1] Ghedamu, M., Watkinson, A. P., and Epstein, N., Mitigation of Wax Build-up on Cold Surfaces, *Fouling Mitigation of Industrial Heat Exchange Equipment*, Begell House, NY, pp. 473–489, 1997.

[2] Rohsenow, W., Hartnett, J., and Cho, Y., *Handbook of Heat Transfer*, McGraw-Hill Education, New York, 1998.

[3] Kitto, J. B., and Robertson, J. M., Effects of Maldistribution of Flow on Heat Transfer Equipment Performance, *Heat Transfer Engineering*, vol. 10, no. 1, pp. 18–25, 1989.

[4] Mueller, A. C., and Chiou, J. P., Review of Various Types of Flow Maldistribution in Heat Exchangers, *Heat Transfer Engineering*, vol. 9, no. 2, pp. 36–50, 1988.

[5] Mueller, A. C., Criteria for Maldistribution in Viscous Flow Coolers, Begel House Inc., 1974.

[6] Putnam, G. R., and Rohsenow, W. M., Viscosity Induced Non-Uniform Flow in Laminar Flow Heat Exchangers, *International Journal of Heat and Mass Transfer*, vol. 28, no. 5, pp. 1031–1038, 1985.

[7] Wonchala, E. P., and Wynnyckyj, J. R., The Phenomenon of Thermal Channelling in Countercurrent Gas-Solid Heat Exchangers, *The Canadian Journal of Chemical Engineering*, vol. 65, no. 5, pp. 736–743, 1987.

[8] Ishiyama, E. M., Paterson, W. R., and Wilson, D. I., Thermo-Hydraulic Channelling in Parallel Heat Exchangers Subject to Fouling, *Chemical Engineering Science*, vol. 63, no. 13, pp. 3400–3410, 2008.

[9] Huang, Z., Lu, Y., Hoffmann, R., Amundsen, L., and Fogler, H. S., The Effect of Operating Temperatures on Wax Deposition, *Energy & Fuels*, vol. 25, no. 11, pp. 5180–5188, 2011.

[10] Mahir, L. H. A., Vilas Bôas Fávero, C., Ketjuntiwa, T., Fogler, H. S., and Larson, R. G., Mechanism of Wax Deposition on Cold Surfaces: Gelation and Deposit Aging, *Energy & Fuels*, vol. 33, no. 5, pp. 3776–3786, 2019.

[11] Paso, K. G., and Fogler, H. S., Bulk Stabilization in Wax Deposition Systems, *Energy and Fuels*, vol. 18, no. 4, pp. 1005–1013, 2004.

[12] Singh, P., Venkatesan, R., Scott Fogler, H., and Nagarajan, N. R., Morphological Evolution of Thick Wax Deposits during Aging, *AIChE Journal*, vol. 47, no. 1, pp. 6–18, 2001.

[13] Ghedamu, M.A., Wax deposition from kerosene onto cooled surfaces, M.A.Sc Thesis, University of British Columbia, 1995.

[14] Gnielinski, V., Heat Transfer Coefficients for Turbulent Flow in Concentric Annular Ducts, *Heat Transfer Engineering*, vol. 30, no. 6, pp. 431–436, 2009.

[15] Bennett, C. A., and Hohmann, R. P., Methods for Calculating Shear Stress at the Wall for Single-Phase Flow in Tubular, Annular, Plate, and Shell-Side Heat Exchanger Geometries, *Heat Transfer Engineering*, vol. 38, no. 9, pp. 829–840, 2017.

[16] Kays, W. M., Numerical Solutions for Laminar Flow Heat Transfer in Circular Tubes, *Trans. ASME*, pp. 1265–1274, 1955.

[17] Yeap, B. L., Wilson, D. I., Polley, G. T., and Pugh, S. J., Mitigation of Crude Oil Refinery Heat Exchanger Fouling through Retrofits Based on Thermo-Hydraulic Fouling Models, *Chemical Engineering Research and Design*, vol. 82, no. 1, pp. 53–71, 2004.